HHS Public Access

Author manuscript

J Immunol. Author manuscript; available in PMC 2018 November 01.

Published in final edited form as:

J Immunol. 2017 November 01; 199(9): 3176–3186. doi:10.4049/jimmunol.1700140.

Aging-Impaired Filamentous Actin Polymerization Signaling Reduces Alveolar Macrophage Phagocytosis of Bacteria

Zhigang Li[*,†], **Yang Jiao**[*,‡], **Erica K. Fan**[§], **Melanie J. Scott**[*], **Yuehua Li**[*,†], **Song Li**[¶], **Timothy R. Billiar**[*,**], **Mark A. Wilson**[*,†], **Xueyin Shi**[‡], and **Jie Fan**[*,†,**]

[*]Department of Surgery, University of Pittsburgh School of Medicine, Pittsburgh, PA 15213

[†]Research and Development, Veterans Affairs Pittsburgh Healthcare System, Pittsburgh, PA 15240

[‡]Department of Anesthesiology, Shanghai Xinhua Hospital, Jiaotong University School of Medicine, Shanghai, China 200092

[§]University of Pittsburgh School of Arts and Science, Pittsburgh, PA 15213

[¶]Center for Pharmacogenetics, Department of Pharmaceutical Sciences, University of Pittsburgh School of Pharmacy, Pittsburgh, PA 15261

[**]McGowan Institute for Regenerative Medicine, University of Pittsburgh, Pittsburgh, PA 15219

Abstract

In elderly patients bacterial infection often causes severe complications and sepsis. Compared to younger patients, older patients are more susceptible to sepsis caused by respiratory infection. Macrophage (Mϕ) phagocytosis of bacteria plays a critical role in the clearance of pathogens and the initiation of immune responses. It has been suggested that Mϕ exhibit age related functional alterations, including reduced chemotaxis, phagocytosis, antibacterial defense, and ability to generate reactive oxygen species. However, the mechanisms behind these changes remain unclear. The current study aimed at determining changes in bacterial phagocytosis in aging alveolar Mϕ (AMϕ) and the underlying mechanisms. We show that bacteria initiate cytoskeleton remodeling in AMϕ through interaction with macrophage receptor with collagenous structure (MARCO), a bacterial scavenger receptor. This remodeling, in turn, promotes enhanced cell surface expression of MARCO and bacterial phagocytosis. We further demonstrate that Rac1-GTP mediates MARCO signaling and activates actin-related protein-2/3 (Arp2/3) complex, a filamentous actin (F-actin) nucleator, thereby inducing F-actin polymerization, filopodia formation, and increased cell surface expression of MARCO, all of which are essential for the execution of bacteria phagocytosis. However, AMϕ isolated from aging mice exhibit suppressed Rac1 mRNA and protein expression,

Correspondence should be addressed to X.S. (shixueyin1128@163.com) or J.F. (jif7@pitt.edu).
Z.L. and Y.J. contributed equally to this work.

Disclosures

The authors have no financial conflicts of interest.

Author Contributions

Z.L., Y.J., E.F., Y.L. planned and did experiments including cell isolation and treatment, confocal microcopy, Western blotting, and flow cytometry; Z.L., Y.L., Y.J. did animal experiments; T.R.B., M.A.W., S.L., X.S., and J.F. planned the project and conceived the experiments; Z.L., E.F., M.J.S., X.S., and J.F. conceived the data and wrote the manuscript.

which resulted in decreases in Rac1-GTP levels and Arp2/3 activation, and subsequent attenuation of F-actin polymerization, filopodia formation and cell surface expression of MARCO. As a result, bacterial phagocytosis in aging AMϕ is decreased. This study highlights a previously unidentified mechanism by which aging impairs Mϕ phagocytosis of bacteria. Targeting these pathways may improve outcomes of bacterial infection in elderly patients.

Introduction

Aging substantially impacts the immune system (1), manifesting as declining or dysregulated immune responses, more severe complications from bacterial infections, reduced vaccine response, and dysfunction of B and T cells (2, 3). Disease resulting from infection constitutes one third of mortality in the global population aged 65 or older (4). Respiratory infections, in particular, carry a high risk of death in elderly patients (5). However, the mechanisms underlying the high susceptibility of aging patients to respiratory infection remain unclear.

Phagocytosis of bacteria by phagocytes is one of the first lines of host defense against pathogen infection and initiates subsequent immune responses (6). Phagocytosis is driven by actin cytoskeleton rearrangements resulting in membrane-bound vacuolar phagosome formation (7–9). Macrophages (Mϕ) play an important role in the rapid clearance of bacteria through phagocytosis of bacteria, therefore preventing bacteria from spreading and multiplying (10). The phagocytosis process involves multiple stages including bacterial survey, phagocytic cup formation, and phagosomal sealing, all of which require actin cytoskeleton remodeling (8, 9).

Mϕ recognition of pathogens depends on recognition of pathogen-associated molecular patterns (PAMPs) by TLRs or scavenger receptors. Eight classes of scavenger receptors have been defined, which are denoted by class A to class I (excluding C) (11). Macrophage receptor with collagenous structure (MARCO, also known as SCARA2 and SR-A2) is a class A scavenger receptor and is important for Mϕ phagocytosis of bacteria (12). MARCO recognizes and binds Gram-negative and Gram-positive bacteria via its scavenger receptor cysteine-rich (SRCR) domain at the extracellular C-terminal, and promotes an innate antimicrobial immune response (13, 14).

Mϕ phagocytosis of bacteria results from actin-based membrane cytoskeleton remodeling processes, which include filopodia and podosome formation and cell membrane ruffling, regulated by actin polymerization (15). Actin filament (F-actin) rearrangement includes F-actin polymerization (nucleation) and branching (16, 17). F-actin branching and extension in Mϕ is regulated by the actin-related protein-2/3 (Arp2/3) complex. Activation of the Arp2/3 complex is regulated by nucleation-promoting factors (NPFs), including Wiskott-Aldrich syndrome protein (WASP) and neural (N)-WASP (18), both of which are expressed in Mϕ and activated by Rho family GTPases including Rac1 and Cdc42 (19), which are reported to be needed for membrane ruffling and phagocytosis in leukocytes (20).

In this study, using a mouse model of pulmonary *E.coli* infection, we show that in AMϕ isolated from aging (>18 months old) mice, Rac1 mRNA expression is lower in alveolar

macrophages from aging mice compared to young mice, which results in decreases in Rac1-GTP level and Arp2/3 activation, as well as downstream attenuation of F-actin polymerization, filopodia formation, and reduced cell surface expression of MARCO. As a result, bacterial phagocytosis in aging AMϕ is decreased and delayed. This study explores a previously unidentified mechanism by which aging impairs Mϕ phagocytosis of bacteria. Targeting related pathways of bacterial phagocytosis may serve as a potential therapeutic strategy for improving outcomes from bacterial infection in the elderly patients.

Materials and Methods

Reagents

Escherichia coli (K-12 strain) BioParticles® Alexa Fluor® 488 conjugate (E13231) was purchased from Thermo Fisher Scientific (Pittsburgh, PA, USA). siNC and siMARCO was purchased from Integrated DNA Technologies (Coralville, IA, USA). Anti-Mouse F4/80 Antigen PE-Cyanine5 (15-4801-80) and anti-Mouse CD284 (TLR4) PE (12-9041-80) were purchased from eBioscience (San Diego, CA, USA). Rat IgG1 PE-conjugated Antibody (IC005P), Mouse MARCO PE-conjugated Antibody (FAB2956P), Rat IgG2A PE-conjugated Antibody (IC006P), Mouse Fc gamma RI/CD64 PE-conjugated Antibody (FAB20741P), and Mouse MARCO Antibody (AF2956-SP) were purchased from R&D Systems. Rac1 inhibitor, NSC23766 (1177865-17-6, Cayman Chemical, Ann Arbor, MI, USA); N-WASP inhibitor, Wiskostatin (253449-04-6, Cayman Chemical); Arp2/3 complex inhibitor, CK666 (SML0006, Sigma-Aldrich, St. Louis, MO, USA); Fascin inhibitor (21), $C_{20}H_{14}F_3N_3O_2$ (L457698-1EA, Sigma-Aldrich). CytoPainter Phalloidin-iFluor 647 Reagent (ab176759) and Anti-Arp2 (phospho T237 + T238) antibody (ab119766) were purchased from abcam (Cambridge, MA, USA). Rac1 and Rac1-GTP detected by Rac1/cdc42 Activation Magnetic Beads Pulldown Assay (17-103-94, EMD Millipore, Kankakee, IL, USA). Arp2 (5614S), N-WASP (4848S), and GAPDH (5174S) antibody from Cell Signaling Technology (Danvers, MA, USA). Lysogeny Broth (LB) (Lennox, L3022) and LB Agar Plates (L5542) were purchased from Sigma-Aldrich. Latex Beads-Rabbit IgG-PE Complex (600541) was purchased from Cayman Chemical.

Animal strains

8 weeks old male (young) C57BL/6 mice were purchased from The Jackson Laboratory (Bar Harbor, ME, USA). Eighteen month old (aging) male C57BL/6 mice were obtained from National Institute on Aging (NIA). TLR4 knockout ($TLR4^{-/-}$) mice were obtained from Dr. Billiar's laboratory at the University of Pittsburgh. All animal experimental protocols were reviewed and approved by the Institutional Animal Care and Use Committees of University of Pittsburgh and VA Pittsburgh Healthcare System.

Intratracheal injection of *E. coli* in mouse

Young or aging mice were anesthetized with ketamine (50 mg/kg B.W.) combined with xylazine (5 mg/kg B.W.). Alexa Fluor 488 conjugated *E. coli* (4×10^8 bacteria cells/kg B.W.) or *E. coli* (strain BL21, 4×10^8 bacteria cells/kg B.W.) in 0.2 ml saline were given via intratracheal aerosol administration using MicroSprayer® aerosolizer high pressure syringe (Penn-Century, Wyndmoor, USA). Sham animals underwent the same anesthesia procedure

and intratracheal aerosol injection of 0.2 ml of saline. Bronchoalveolar lavage fluid (BALF) was collected and the alveolar macrophages (AMϕ) were isolated for further analysis.

AMϕ isolation and culture

Red blood cells (RBC) in BALF were lysed by RBC lysis buffer (eBioscience), and remaining cells were concentrated and resuspended in Dulbecco's Modified Eagle Medium (DMEM) containing 10% FBS supplemented with 50 μg/ml penicillin/streptomycin. AMϕ were plated at 1×10^6 cells/ml and allowed to adhere for 45 min, then washed to remove non-adherent cells (22).

Flow cytometry

AMϕ were treated with or without Alexa Fluor 488-conjugated *E. coli* or non-fluorescently labelled *E. coli*, and were stained with PECy5-F4/80 (a pan macrophage marker), or PE-MARCO, Rat IgG1 PE-conjugated-antibody (used as PE-MARCO isotype control), or PE-FcγRI, Rat IgG2A PE-conjugated-antibody (used as PE-FcγRI isotype control), followed by analysis by BD FASC flow cytometer. The mean fluorescence intensity (MFI) was calculated by flowjo v10.0.

Confocal immunofluorescence

The AMϕ, which were collected from young and aging mice, were seeded in a glass bottomed petri dish (P35G-0-10-C, MatTek Corporation, Ashland, MA, USA) and fixed with 4% paraformaldehyde for 15 min at room temperature. After washing with PBS, cells were permeabilized with 0.01% Triton X-100 in PBS for 15 min at room temperature, followed by blocking with 5% bovine serum albumin in PBS for 1h at room temperature. The cells were stained with phalloidin for 60 min or were incubated with primary antibody (MARCO or p-Arp2) at 4°C overnight, followed by incubation with Alexa Fluor 488 or Cy3-conjugated secondary antibody for 1 h at room temperature. To stain the F-actin, the cells were incubated with iFluor 647-conjugated phalloidin. Cell nucleus was stained with Hoechst 33258 (Sigma-Aldrich). The AMϕ were then analyzed by confocal microscopy (Olympus, Fluoview-FV1000, Olympus America Co.) and data collected across three random fields in each independent experiments. To analyze the number of filopodia per cell, we outlined the cytoskeleton (phalloidin staining) and counted the numbers of spike-like phalloidin staining using ImageJ version 1.50i. We then quantified the co-localization of p-Arp2 and phalloidin by Pearson's coefficient using ImageJ version 1.50i.

Western Blot

BMDM lysates were separated by 12% and 15% SDS-PAGE, and then transferred onto PVDF membranes. After blocking for 1h at room temperature with blocking buffer (LI-COR Biosciences, Lincoln, NE, USA), blots were incubated with primary antibody (Rac1, p-Arp2, t-Arp2, N-WASP, or GAPDH), at 4°C overnight, followed by incubation with appropriate secondary antibodies (LI-COR Biosciences) for 1h. Protein bands were detected using the Odyssey System from LI-COR Biosciences, and quantified using ImageJ version 1.50i.

RNA extraction and quantitative real-time PCR

Plated cells were harvested and total RNA isolated using TRIzol® RNA Isolation Reagents (Thermo Fisher Scientific, Pittsburgh, PA, USA) following manufacturer's instructions. Real-time RT-PCR was done using iTaq™ Universal SYBR® Green Supermix (1725121, Bio-Rad) in a Bio-Rad iQ5 real time PCR machine (Bio-Rad). The following gene-specific primers were used for amplifying genes: *Rac1* forward, 5'-GAGACGGAGCTGTTGGTAAAA-3', reverse, 5'- ATAGGCCCAGATTCACTGGTT-3'; and *18S* forward, 5'-GTAACCCGTTGAACCCCATT-3', reverse, 5'-CCATCCAATCGGTAGTAGCG-3'. Reverse transcription was performed using iScript™ Reverse Transcription Supermix (170-8840, Bio-Rad) following the manufacturer's instructions. Amplification was performed with cycling conditions of 95°C for 15s then 60°C for 30s for 40 cycles. After the amplification protocol was completed, PCR product was subjected to melt-curve analysis using Bio-Rad iQ5 software (Bio-Rad). Fold change was calculated using the ΔΔ threshold cycle method (23) and the value for the 18s rRNA gene, which was normalized to untreated groups.

Statistical Analysis

The data are presented as mean ± SEM of the indicated number of experiments/repeats. All image graphs were counting by three random fields in three independent experiments. SPSS 20.0 or GraphPad Prism v.6.0 was used for statistical analysis. Significances between groups were determined by using one-way ANOVA, two-way ANOVA, or independent-sample two-tailed Student's *t*-test, and a significance level of $p < 0.05$ was considered as statistically significant.

Results

Aging impairs AMϕ phagocytosis of *E. coli*

To determine differences in AMϕ phagocytosis of *E. coli* between young and aging mice, young (8 weeks old) and aging (18 months old) mice were intratracheally (i.t.)-injected with Alexa Fluor 488-conjugated *E. coli*, AMϕ were collected from BALF, and numbers of intra-AMϕ fluorescent bacteria were measured at 1 h after injection. Figure 1A shows that phagocytosis of *E. coli* in aging AMϕ was significantly decreased as compared with young AMϕ (MFI was 11.35±2.03 in the aging versus 139.67±27.38 in the young, $p<0.01$). Whereas 50% of alveolar macrophages from young mice had *E. coli* associated with them, only 5% of macrophages from old mice bound or internalized *E. coli*. (Figure 1B). To further compare bacteria clearance capacity between young and aging AMϕ, we administered non-fluorescently labelled live *E. coli* (i.t.) to the young and aging mice, and at 2 h after bacteria administration, BAL fluid was collected and bacterial numbers analyzed by bacterial colony forming test. As shown in Figure 1C, colony formation from the BALF of aging mice was statistically significantly greater than that from young mice, indicating bacteria clearance capacity in aging mice was significantly weakened. *In vitro* studies were also performed. AMϕ were isolated from young and aging mice, respectively, and then treated with the Alexa Fluor 488-conjugated *E. coli* for up to 120 min *in vitro*. As shown in Figure 1D, the phagocytosis of *E. coli* in aging AMϕ was significantly decreased at 60 min to 120 min after bacteria treatment, as compared with young AMϕ. We also visualized

phagocytosis of *E. coli* in young and aging AMϕ, as shown in Figure 1E. The number of AMϕ that phagocytosed *E. coli* was markedly decreased in aging AMϕ as compared with young AMϕ. Collectively, these data indicate that aging impaired AMϕ phagocytosis of *E. coli*.

Upregulated MARCO cell surface expression is required for AMϕ phagocytosis of *E. coli*

MARCO is a class A scavenger receptors, which has been shown to be important in bacterial phagocytosis (12). We first determined the differences in MARCO cell surface expression between young and aging AMϕ. As shown in Figure 2A, there was no difference in the level of MARCO expression at baseline between young and aging AMϕ, however, *E. coli* induced an increase in MARCO cell surface expression in young AMϕ. Whereas, the degree of the increase in aging AMϕ was significantly lower at 60 min after *E. coli* treatment. To visualize MARCO distribution in young and aging AMϕ, we stained MARCO with Alexa Fluor 488 in young and aging AMϕ collected at 0–60 min after *E. coli* treatment. Figure 2B shows *E. coli*-induced MARCO re-distribution on the cell surface in young AMϕ, but not in aging AMϕ, at 60 min after *E. coli* treatment. To further investigate the role of MARCO in *E. coli* phagocytosis, we knocked down MARCO in AMϕ by transfection of small interfering RNA against MARCO (siMARCO). As shown in Figure 2C, MARCO protein expression was significantly diminished in the AMϕ transfected with siMARCO. MARCO knockdown resulted in a significant decrease in MARCO cell surface expression in young AMϕ treated with or without *E. coli* (Figure 2D), and MARCO knockdown also led to a decrease in AMϕ phagocytosis of Alexa Fluor 488-conjugated *E. coli* (Figure 2E). To determine whether the change in MARCO expression in AMϕ following *E. coli* treatment is specific, we also measured the change of macrophage surface expression of FcγRI, which is a member of immunoglobulin superfamily and plays a role in recognizing and phagocytosing microbes, following *E. coli* treatment. We found that *E. coli* did not increase the FcγRI cell surface expression in AMϕ (Figure 2F). Furthermore, siMARCO did not change the macrophage phagocytosis of IgG-coated latex beads, which is mediated through Fc receptor (Figure 2G). These results indicate that *E. coli*-induced MARCO cell surface expression in AMϕ is a specific event and is required for the AMϕ phagocytosis of *E. coli*.

Actin polymerization signaling mediates MARCO cell surface expression and phagocytosis of *E. coli*

F-actin polymerization is believed to be important for cell phagocytosis (24). To determine the role of the F-actin polymerization in inducing MARCO cell surface expression and AMϕ bacteria phagocytosis, we blocked the signaling pathway that regulates F-actin polymerization by using pharmacological inhibitors targeting Rac1 (NSC23766), N-WASP (Wiskostatin), and Arp2/3 complex (CK666). We selected a time point at 60 min after *E. coli* treatment based on the observation that phagocytosis of *E. coli* in young AMϕ was rapidly initiated at as early as 15 min after *E. coli* treatment, and peaked at 60 min (Figure 3A). As shown in Figure 3B and 3C, inhibition of Rac1, N-WASP, or Arp2/3 complex significantly decreased MARCO cell surface expression in AMϕ (Figure 3B), and diminished phagocytosis of *E. coli* (Figure 3C). These results indicate that MARCO cell surface expression and phagocytosis of *E. coli* depend on the Rac1-N-WASP-Arp2/3 complex signaling known to regulate F-actin polymerization.

Aging impairs AMϕ filopodia formation and decreases phagocytosis of *E. coli*

Filopodia formation in phagocytes is believed to be critical for execution of bacterial phagocytosis. Filopodia are thin (0.1–0.3 μm), spike-like protrusions that contain bundles of actin filaments (F-actin) (25). Filopodia survey phagocytic targets in the extracellular environment (26). Therefore, filopodia can be a marker of F-actin polymerization and cytoskeleton remodeling. To visualize filopodia formation in AMϕ, we treated young AMϕ with *E. coli* and the spikes of F-actin, which was stained with phalloidin, were counted using confocal microscope. AMϕ were also treated with TLR2 ligand bacterial lipoprotein (BLP, 1 μg/ml) and TLR4 ligand lipopolysaccharide (LPS, 1 μg/ml) to serve as positive controls. As shown in Figure 4A, *E. coli*, BLP, and LPS stimulated AMϕ to form filopodia, and there was no statistically significant difference between the numbers of AMϕ filopodia formed after induction by *E. coli*, BLP, or LPS.

To determine the changes in the ability to form filopodia in aging AMϕ, young and aging mice were subjected to *E. coli* i.t., and at 0.5 h after *E. coli* i.t., AMϕ were isolated from BAL fluid, and filopodia formation in the AMϕ was visualized by confocal microscopy with phalloidin staining. Figure 4B shows that *E. coli* induced filopodia formation in young AMϕ, but not in aging AMϕ. *In vitro* time course studies also supported that *E. coli*-induced filopodia formation was significantly decreased in aging AMϕ, as compared with that in young AMϕ (Figure 4C).

To further determine whether TLR4 signaling is involved in mediating the age-specific changes in *E. coli*-induced filopodia formation, we first measured AMϕ surface expression of TLR4 in young and aging mice. *E. coli* challenge did not induce a difference in macrophage surface expression of TLR4 between young and aging AMϕ (Figure S1A). We then determined the effect of TLR4 deficiency on AMϕ phagocytosis of *E. coli* using $TLR4^{-/-}$ AMϕ. $TLR4^{-/-}$ did not effect the *E. coli*-induced filopodia formation in AMϕ (Figure S1B) as well as phagocytosis of *E. coli* (Figure S1C and S1D). Furthermore, we treated AMϕ collected from young and aging mice with a variety of concentrations of LPS, and found that LPS-induced macrophage filopodia formation requires a high dose of LPS (1,000 ng/ml), this does not differ between young and aging mice (Figure 4D).

To evaluate the impact of impaired filopodia formation in aging AMϕ, we further verified the importance of filopodia formation in AMϕ phagocytosis of *E. coli*. We pretreated AMϕ with fascin inhibitor prior to *E. coli* stimulation. Fascin is an actin-binding protein that regulates filopodia formation (27, 28). Inhibition of fascin significantly reduced both filopodia formation in AMϕ (Figure 4E) and phagocytosis of *E. coli* (Figure 4F).

To determine the role of F-actin polymerization in the filopodia formation, inhibitors NSC23766, Wiskostatin, or CK666 were added to AMϕ 30 min before *E. coli* treatment. Treatment with any of these inhibitors significantly decreased *E. coli*-induced filopodia formation (Figure 4G).

Aging suppresses Rac1 expression and decreases Rac1-GTP level

The results described above suggest impaired actin polymerization signaling in aging. To identify aging effects on this signaling pathway, we measured mRNA and protein expression

of N-WASP, Arp2/3, and Rac1. We found that Rac1 mRNA expression and protein expression of its activated form, Rac1-GTP, were significantly decreased in aging AMϕ (Figure 5A). As shown in Figure 5A and 5B, the basal level of Rac1 mRNA and protein in aging AMϕ was also significantly lower than that in young AMϕ. *E. coli* induced an increase in the Rac1-GTP level in young AMϕ, but failed to increase the Rac1-GTP level in aging AMϕ (Figure 5B). In addition, *E. coli* induced Arp2 phosphorylation, an indication of Arp2/3 complex activation, in young AMϕ, but was significantly attenuated in aging AMϕ (Figure 5C). The level of N-WASP expression was not significantly different between young AMϕ and aging AMϕ in both basal and *E. coli*-treated conditions (Figure 5D). In order to determine whether decreased phosphorylation of Arp2 is responsible for the decreased phalloidin formation in aging AMϕ, we detected colocalization of phosphorylated Arp2 and phalloidin. As shown in Figure 5E, *E. coli* induced colocalization of phosphorylated Arp2 and phalloidin in young AMϕ within 30 min but this was significantly attenuated in aging AMϕ (Figure 5E). Similarly, *in vivo E. coli* i.t. induced colocalization of phosphorylated Arp2 and phalloidin in AMϕ isolated from young mice, but not from aging mice (Figure 5F).

Taken together, these data suggest that Rac1 expression in aging AMϕ is suppressed, which leads to decreases in Rac1-GTP levels and Arp2/3 activation, followed by attenuation of F-actin polymerization and filopodia formation.

Discussion

There is an increased prevalence of infections with age (29). Marrie *et. al* reported that there is a 3 fold increase in community-acquired pneumonia in the elderly population (30). However, the mechanism by which aging leads to increased susceptibility to bacterial infection has not been fully elucidated. Bacteria have a very rapid growth rate. The generation time for *E. coli*, defined as the time period during which bacteria double their number, is 15–20 minutes (31, 32). Delayed host cell phagocytosis of bacteria can lead to infection propagation and even the development of sepsis and multi-organ failure (10, 33). Our current study shows that in aging AMϕ, Rac1 mRNA expression is lower in alveolar macrophages from aging mice compared to young mice, which then leads to decreased Rac1-GTP level and Arp2/3 activation, followed by attenuation of F-actin polymerization, filopodia formation, and cell surface expression of MARCO. As a result, bacterial phagocytosis in aging AMϕ is decreased and delayed. This study explored a previously unidentified mechanism by which aging impairs Mϕ phagocytosis of bacteria.

Aging is a complex process that results in many changes in physiological processes that ultimately increase susceptibility to a wide range of diseases (34, 35). Numerous transcriptional changes have been reported in aging, which result in multiple genotype variations, declining organ function, and shorter lifespan (36, 37). Large scale age-related gene expression studies showed that the changes in immune responses with aging are closely related to gene expression in multiple organs. For example, decreases in the expression of immune-related genes in spleen were suggested to be responsible for the decrease in immune responses in aging (36, 38, 39). Our current study reveals a new causal role for deficits in transcriptional expression of Rac1 in diminished AMϕ phagocytosis of *E. coli* in

aging. This finding adds to the importance of transcriptional changes in the mechanisms of aging-related diseases.

MARCO functions as a critical *E. coli* scavenger receptor (40). Our study supports the important role of MARCO in *E. coli* phagocytosis, since knockdown of MARCO significantly decreased AMϕ *E. coli* phagocytosis. Interestingly, as shown by others and our current study, MARCO cell surface expression in AMϕ is initiated by bacteria (12, 41). We observed an increase in MARCO cell surface expression during phagocytosis of bacteria in this study. We also measured the change of macrophage surface expression of FcγRI, which is a member of the immunoglobulin superfamily that also plays a role in recognizing and phagocytosing microbes, following *E. coli* treatment. We found that *E. coli* did not increase FcγRI cell surface expression in AMϕ. This result suggests that the observed alterations in MARCO and its role in macrophage phagocytosis of *E. coli* are quite specific. We believe that other receptors might also be involved in *E. coli* phagocytosis. However, our current study shows that MARCO is, at least, one of the important receptors that mediate macrophage phagocytosis of bacteria. More importantly, the underlying mechanism for the decrease of macrophage phagocytosis of bacteria in aging mice is the decrease of Rac1 expression and subsequent impaired filamentous actin polymerization. The degree of MARCO specificity therefore does not alter this concluded age-dependent mechanism.

Cytoskeleton remodeling is required for cell surface receptor compartmentalization, clustering, exposure, and signaling transduction (8, 42–44). Our results show that F-actin polymerization induces cytoskeleton remodeling and facilitates MARCO cell surface expression, which in turn enhances AMϕ phagocytosis of *E. coli*. However, in aging AMϕ, the down regulation of Rac1 weakened F-actin polymerization signaling, and thus failed to increase MARCO cell surface expression, and subsequent effective phagocytosis.

The filopodia on macrophages are cellular tentacles that survey the environment and assist with uptake of extracellular pathogens (25, 45, 46). The current study shows that inhibition of F-actin polymerization signaling using inhibitors targeting Rac1, N-WASP, and Arp2/3 complex significantly decreases filopodia formation during phagocytosis of *E. coli*, indicating that the filopodia formation depends on cytoskeleton remodeling as well. However, the down regulation of Rac1 expression in aging impairs filopodia formation, which serves as another mechanism underlying decreased bacterial phagocytosis in aging. A direct result of decreased AMϕ phagocytosis of bacteria is an increase in the number of bacteria in the lung, which would lead to bacterial spread and more severe pulmonary infection. We demonstrated that pulmonary bacteria colony formation, as an indication of pulmonary bacteria clearance ability, significantly increased in aging animals, which suggests an important pathological consequence following impairment of AMϕ phagocytosis of bacteria.

In summary, this study demonstrates a novel mechanism underlying aging-impaired AMϕ phagocytosis of *E. coli*. F-actin polymerization signaling mediated MARCO cell surface expression and filopodia formation, both of which are critical for execution of phagocytosis of bacteria. However, the deficit in Rac1 transcriptional expression in aging AMϕ leads to the decrease in Rac1-GTP level and Arp2/3 activation, followed by attenuation of F-actin

polymerization and the consequent decrease in bacterial phagocytosis. This study explores a previously unidentified mechanism by which aging impairs Mϕ phagocytosis of bacteria. Targeting these phagocytosis pathways may serve as a potential therapeutic strategy for improving outcomes of bacterial infection in elderly patients.

Supplementary Material

Refer to Web version on PubMed Central for supplementary material.

Acknowledgments

Grant support

This work was supported by the National Institutes of Health Grant R01-HL-079669 (J.F. and M.A.W.), National Institutes of Health Grant R56-HL-123882 (J.F.), National Institutes of Health Grant R01HL076179-09 (J.F.), VA Merit Award 1I01BX002729 (J.F.), National Natural Science Foundation of China 81470262 (J.F.), Key Program of Medical Science Development of PLA BWS12J027 (X.S.), National Natural Science Foundation of China 81372103 (X.S.), National Natural Science Foundation of China 81671944 (X.S.), and National Institutes of Health Grant R01GM102146 (M.J.S).

Abbreviations used in this article

AMϕ	alveolar macrophages
Arp2/3	actin-related protein 2/3
BMDM	bone marrow derived-macrophages
E. coli	*Escherichia coli*
F-actin	filamentous actin
MARCO	macrophage receptor with collagenous structure
Mϕ	macrophages
MOI	Multiplicity of infection
N-WASP	neural Wiskott-Aldrich syndrome protein
TLR4	toll-like receptor 4

References

1. Montgomery RR, Shaw AC. Paradoxical changes in innate immunity in aging: recent progress and new directions. J Leukoc Biol. 2015; 98:937–943. [PubMed: 26188078]
2. Frasca D, Blomberg BB. B cell function and influenza vaccine responses in healthy aging and disease. Curr Opin Immunol. 2014; 29:112–118. [PubMed: 24934648]
3. Goronzy JJ, Weyand CM. Understanding immunosenescence to improve responses to vaccines. Nat Immunol. 2013; 14:428–436. [PubMed: 23598398]
4. Kline KA, Bowdish DM. Infection in an aging population. Curr Opin Microbiol. 2016; 29:63–67. [PubMed: 26673958]
5. Meyer KC. Lung infections and aging. Ageing Res Rev. 2004; 3:55–67. [PubMed: 15163102]
6. Aderem A. Phagocytosis and the inflammatory response. J Infect Dis. 2003; 187(Suppl 2):S340–345. [PubMed: 12792849]

7. Ernst JD. Bacterial inhibition of phagocytosis. Cell Microbiol. 2000; 2:379–386. [PubMed: 11207593]
8. Freeman SA, Grinstein S. Phagocytosis: receptors, signal integration, and the cytoskeleton. Immunol Rev. 2014; 262:193–215. [PubMed: 25319336]
9. May RC, Machesky LM. Phagocytosis and the actin cytoskeleton. J Cell Sci. 2001; 114:1061–1077. [PubMed: 11228151]
10. Allen LA, Schlesinger LS, Kang B. Virulent strains of Helicobacter pylori demonstrate delayed phagocytosis and stimulate homotypic phagosome fusion in macrophages. J Exp Med. 2000; 191:115–128. [PubMed: 10620610]
11. Canton J, Neculai D, Grinstein S. Scavenger receptors in homeostasis and immunity. Nat Rev Immunol. 2013; 13:621–634. [PubMed: 23928573]
12. van der Laan LJ, Dopp EA, Haworth R, Pikkarainen T, Kangas M, Elomaa O, Dijkstra CD, Gordon S, Tryggvason K, Kraal G. Regulation and functional involvement of macrophage scavenger receptor MARCO in clearance of bacteria in vivo. J Immunol. 1999; 162:939–947. [PubMed: 9916718]
13. Novakowski KE, Huynh A, Han S, Dorrington MG, Yin C, Tu Z, Pelka P, Whyte P, Guarne A, Sakamoto K, Bowdish DM. A naturally occurring transcript variant of MARCO reveals the SRCR domain is critical for function. Immunol Cell Biol. 2016; 94:646–655. [PubMed: 26888252]
14. Elomaa O, Sankala M, Pikkarainen T, Bergmann U, Tuuttila A, Raatikainen-Ahokas A, Sariola H, Tryggvason K. Structure of the human macrophage MARCO receptor and characterization of its bacteria-binding region. J Biol Chem. 1998; 273:4530–4538. [PubMed: 9468508]
15. Pollard TD, Blanchoin L, Mullins RD. Molecular mechanisms controlling actin filament dynamics in nonmuscle cells. Annu Rev Biophys Biomol Struct. 2000; 29:545–576. [PubMed: 10940259]
16. Greenberg S, Burridge K, Silverstein SC. Colocalization of F-actin and talin during Fc receptor-mediated phagocytosis in mouse macrophages. J Exp Med. 1990; 172:1853–1856. [PubMed: 2124254]
17. Greenberg S. Signal transduction of phagocytosis. Trends Cell Biol. 1995; 5:93–99. [PubMed: 14732162]
18. Goley ED, Welch MD. The ARP2/3 complex: an actin nucleator comes of age. Nat Rev Mol Cell Biol. 2006; 7:713–726. [PubMed: 16990851]
19. Aspenstrom P, Lindberg U, Hall A. Two GTPases, Cdc42 and Rac, bind directly to a protein implicated in the immunodeficiency disorder Wiskott-Aldrich syndrome. Curr Biol. 1996; 6:70–75. [PubMed: 8805223]
20. Cox D, Chang P, Zhang Q, Reddy PG, Bokoch GM, Greenberg S. Requirements for both Rac1 and Cdc42 in membrane ruffling and phagocytosis in leukocytes. J Exp Med. 1997; 186:1487–1494. [PubMed: 9348306]
21. Huang FK, Han S, Xing B, Huang J, Liu B, Bordeleau F, Reinhart-King CA, Zhang JJ, Huang XY. Targeted inhibition of fascin function blocks tumour invasion and metastatic colonization. Nat Commun. 2015; 6:7465. [PubMed: 26081695]
22. Zhang X, Goncalves R, Mosser DM. The isolation and characterization of murine macrophages. Curr Protoc Immunol Chapter. 2008; 14 Unit 14 11.
23. Livak KJ, Schmittgen TD. Analysis of relative gene expression data using real-time quantitative PCR and the 2(−Delta Delta C(T)) Method. Methods. 2001; 25:402–408. [PubMed: 11846609]
24. Rougerie P, Miskolci V, Cox D. Generation of membrane structures during phagocytosis and chemotaxis of macrophages: role and regulation of the actin cytoskeleton. Immunol Rev. 2013; 256:222–239. [PubMed: 24117824]
25. Kress H, Stelzer EH, Holzer D, Buss F, Griffiths G, Rohrbach A. Filopodia act as phagocytic tentacles and pull with discrete steps and a load-dependent velocity. Proc Natl Acad Sci U S A. 2007; 104:11633–11638. [PubMed: 17620618]
26. Nemethova M, Auinger S, Small JV. Building the actin cytoskeleton: filopodia contribute to the construction of contractile bundles in the lamella. J Cell Biol. 2008; 180:1233–1244. [PubMed: 18362182]

27. Yang S, Huang FK, Huang J, Chen S, Jakoncic J, Leo-Macias A, Diaz-Avalos R, Chen L, Zhang JJ, Huang XY. Molecular mechanism of fascin function in filopodial formation. J Biol Chem. 2013; 288:274–284. [PubMed: 23184945]
28. Vignjevic D, Kojima S, Aratyn Y, Danciu O, Svitkina T, Borisy GG. Role of fascin in filopodial protrusion. J Cell Biol. 2006; 174:863–875. [PubMed: 16966425]
29. Gavazzi G, Krause KH. Ageing and infection. Lancet Infect Dis. 2002; 2:659–666. [PubMed: 12409046]
30. Marrie TJ. Community-acquired pneumonia in the elderly. Clin Infect Dis. 2000; 31:1066–1078. [PubMed: 11049791]
31. Harvey JD. Parameters of the generation time distribution of Escherichia coli B-r. J Gen Microbiol. 1972; 70:109–114. [PubMed: 4557385]
32. Plank LD, Harvey JD. Generation time statistics of Escherichia coli B measured by synchronous culture techniques. J Gen Microbiol. 1979; 115:69–77. [PubMed: 393798]
33. Costa-Hurtado M, Ballester M, Galofre-Mila N, Darji A, Aragon V. VtaA8 and VtaA9 from Haemophilus parasuis delay phagocytosis by alveolar macrophages. Vet Res. 2012; 43:57. [PubMed: 22839779]
34. Childs BG, Durik M, Baker DJ, van Deursen JM. Cellular senescence in aging and age-related disease: from mechanisms to therapy. Nat Med. 2015; 21:1424–1435. [PubMed: 26646499]
35. Rojas M, Mora AL, Kapetanaki M, Weathington N, Gladwin M, Eickelberg O. Aging and Lung Disease. Clinical Impact and Cellular and Molecular Pathways. Ann Am Thorac Soc. 2015; 12:S222–227. [PubMed: 26653202]
36. Park SK, Kim K, Page GP, Allison DB, Weindruch R, Prolla TA. Gene expression profiling of aging in multiple mouse strains: identification of aging biomarkers and impact of dietary antioxidants. Aging Cell. 2009; 8:484–495. [PubMed: 19555370]
37. Fushan AA, Turanov AA, Lee SG, Kim EB, Lobanov AV, Yim SH, Buffenstein R, Lee SR, Chang KT, Rhee H, Kim JS, Yang KS, Gladyshev VN. Gene expression defines natural changes in mammalian lifespan. Aging Cell. 2015; 14:352–365. [PubMed: 25677554]
38. Zahn JM, Sonu R, Vogel H, Crane E, Mazan-Mamczarz K, Rabkin R, Davis RW, Becker KG, Owen AB, Kim SK. Transcriptional profiling of aging in human muscle reveals a common aging signature. PLoS Genet. 2006; 2:e115. [PubMed: 16789832]
39. Jonker MJ, Melis JP, Kuiper RV, van der Hoeven TV, Wackers PF, Robinson J, van der Horst GT, Dolle ME, Vijg J, Breit TM, Hoeijmakers JH, van Steeg H. Life spanning murine gene expression profiles in relation to chronological and pathological aging in multiple organs. Aging Cell. 2013; 12:901–909. [PubMed: 23795901]
40. Elomaa O, Kangas M, Sahlberg C, Tuukkanen J, Sormunen R, Liakka A, Thesleff I, Kraal G, Tryggvason K. Cloning of a novel bacteria-binding receptor structurally related to scavenger receptors and expressed in a subset of macrophages. Cell. 1995; 80:603–609. [PubMed: 7867067]
41. Mukouhara T, Arimoto T, Cho K, Yamamoto M, Igarashi T. Surface lipoprotein PpiA of Streptococcus mutans suppresses scavenger receptor MARCO-dependent phagocytosis by macrophages. Infect Immun. 2011; 79:4933–4940. [PubMed: 21986627]
42. Jaqaman K, Grinstein S. Regulation from within: the cytoskeleton in transmembrane signaling. Trends Cell Biol. 2012; 22:515–526. [PubMed: 22917551]
43. Mattila PK, Batista FD, Treanor B. Dynamics of the actin cytoskeleton mediates receptor cross talk: An emerging concept in tuning receptor signaling. J Cell Biol. 2016; 212:267–280. [PubMed: 26833785]
44. Oliver JM, Berlin RD. Cytoskeleton-membrane interaction and the remodeling of the cell surface during phagocytosis and chemotaxis. Adv Exp Med Biol. 1982; 155:113–131. [PubMed: 7158474]
45. Mattila PK, Lappalainen P. Filopodia: molecular architecture and cellular functions. Nat Rev Mol Cell Biol. 2008; 9:446–454. [PubMed: 18464790]
46. Moller J, Luhmann T, Chabria M, Hall H, Vogel V. Macrophages lift off surface-bound bacteria using a filopodium-lamellipodium hook-and-shovel mechanism. Sci Rep. 2013; 3:2884. [PubMed: 24097079]

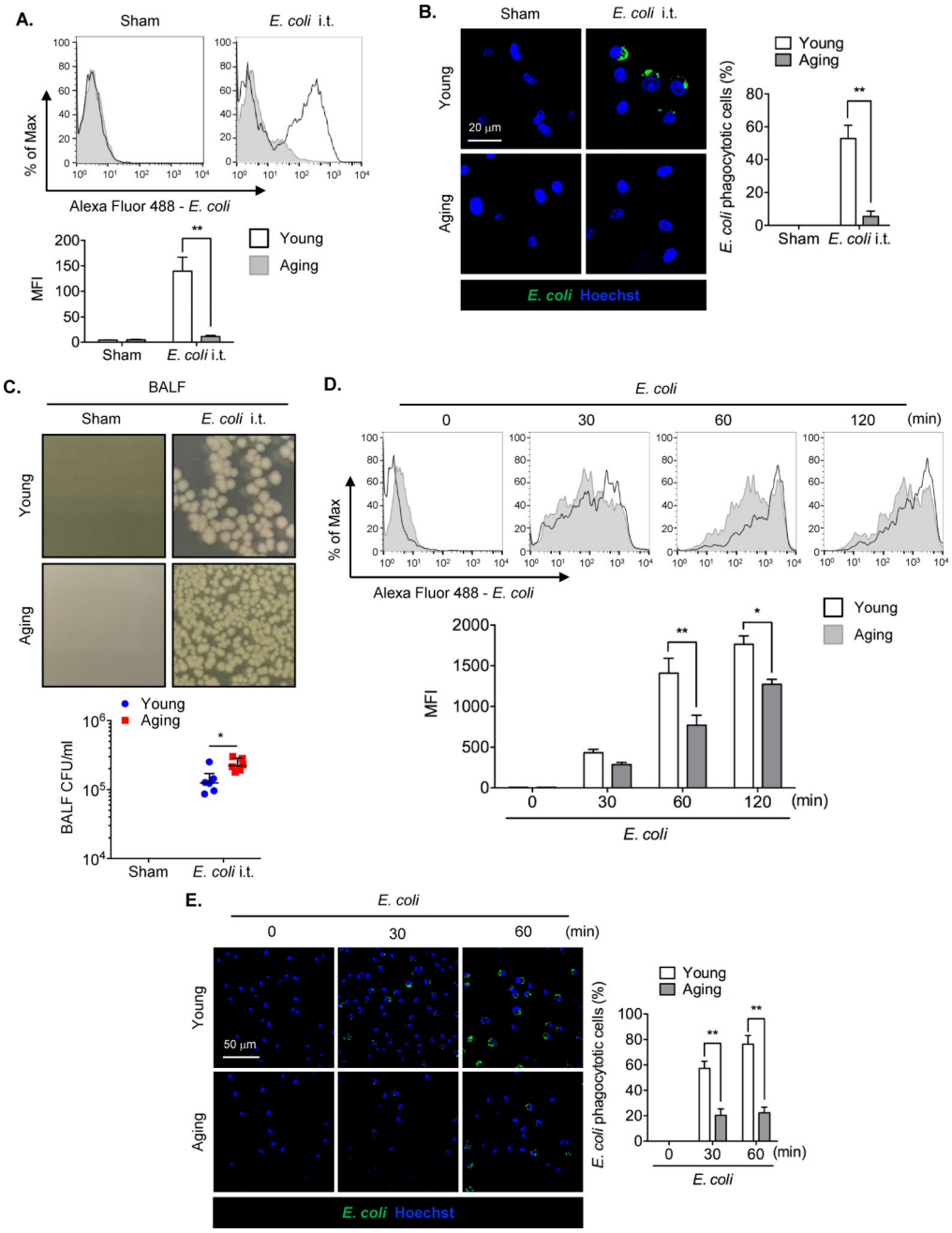

Figure 1. Aging impairs AMϕ phagocytosis of *E. coli*

(**A** and **B**) Uptake of Alexa Fluor 488 conjugated *E. coli* in AMϕ collected from BALF from young or aging mice at 1 h after *E. coli* administration (4×10^8 bacteria cells/kg B.W., i.t.). (**A**) F4/80 positive cells were analyzed by flow cytometry and phagocytosis of *E. coli* was measured by mean fluorescence intensity (MFI). The graph shows mean ± SEM of MFI, n=3, Statistical analysis using two-way ANOVA, Interaction $p = 0.0016$. Tukey's multiple comparisons test shows that *E. coli* i.t./Young vs. *E. coli* i.t./Aging, $p = 0.0008$. **(B)** Confocal microscopy of Alexa Fluor 488-conjugated *E. coli* (green) taken up by AMϕ. The graph shows mean ± SEM of percentage (%) of the AMϕ that phagocytosed *E. coli*, n=3.

Statistical analysis using two-way ANOVA, Interaction $p = 0.0006$. Tukey's multiple comparisons test shows that *E. coli* i.t./Young vs. *E. coli* i.t./Aging, $p = 0.0003$. (**C**) Pulmonary *E. coli* bacterial levels [colony forming units (CFU/ml)]. Young and aging mice were administered *E. coli* (strain BL21, 4×10^8 bacteria cells/kg B.W., i.t.), and at 2 h after treatment, BALF was collected from the mice. The bacteria CFU/ml of BALF were calculated. The graph shows median with interquartile range of BALF CFU/ml, n=6. Statistical analysis using independent-samples Mann-Whitney U test, *E. coli* i.t./Young vs. *E. coli* i.t./Aging $p = 0.026$. (**D**) *In vitro* uptake of Alexa Fluor 488-conjugated *E. coli* [multiplicity of infection (MOI) =4] by AMϕ for time points up to 120 min harvested from young or aging mice and analyzed by flow cytometry and calculated by MFI. The graph shows mean ± SEM of Alexa Fluor 488-conjugated *E. coli* MFI, n=3. Statistical analysis using two-way ANOVA, Interaction $p = 0.0099$. Tukey's multiple comparisons test shows that 60min/Young vs. 60min/Aging, $p = 0.0027$; 120min/Young vs. 120min/Aging, $p = 0.0254$. (**E**) Confocal images showed young or aging AMϕ treated with Alexa Fluor 488-conjugated *E. coli* (MOI=4) for 0 to 60 min. The graph shows mean ± SEM of percentage (%) of the AMϕ that phagocytosed *E. coli*, n=3. Statistical analysis using two-way ANOVA, Interaction $p = 0.0002$. Tukey's multiple comparisons test shows that 30min/Young vs. 30min/Aging, $p = 0.0010$; 60min/Young vs. 60min/Aging, $p < 0.0001$. The asterisks indicate that $*p < 0.05$ or $**p < 0.01$.

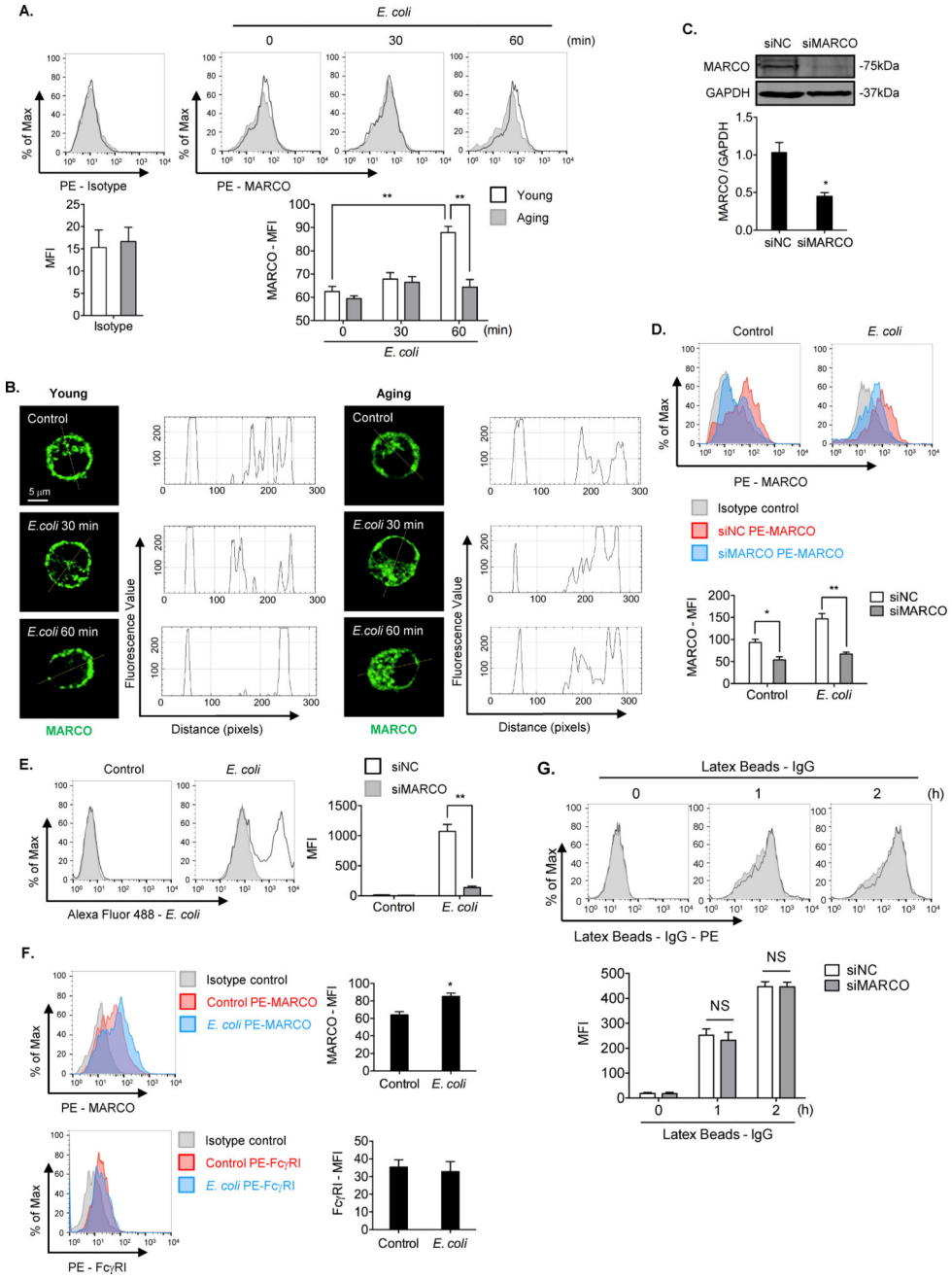

Figure 2. Upregulated MARCO cell surface expression is required for AMϕ phagocytosis of *E. coli*

(**A**) Young and aging AMϕ were treated with Alexa Fluor 488-conjugated *E. coli* (MOI=4) for up to 60 min. Cell surface MARCO stained with PE-MARCO antibody was measured by flow cytometry and expressed as mean fluorescence intensity (MFI). PE-Isotype staining was used as staining control. The graph shows mean ± SEM of MFI, n=3. Statistical analysis using two-way ANOVA, Interaction $p = 0.0014$. Tukey's multiple comparisons test shows that 0min/Young vs. 60min/Young, $p = 0.0001$; 60min/Young vs. 60min/Aging, $p = 0.0003$. (**B**) Young and aging AMϕ were treated with *E. coli* (strain BL21, MOI=4) for up to 60 min. Confocal immunofluorescence images show MARCO staining. The MARCO distribution in

AMϕ was analyzed by software Image J. (**C**) AMϕ were transfected with non-specific small interfering RNA (siNC) or small interfering RNA against MARCO (siMARCO) for 36 h. Total MARCO expression was measured by Western Blot. The graph shows the mean ± SEM of intensity of MARCO/GAPDH, n=3. Statistical analysis using independent-samples two-tailed Student's *t*-test. siNC vs. siMARCO, $p < 0.01$. (**D**) AMϕ were transfected with siNC or siMARCO for 36 h, and then were treated with *E. coli* (MOI=4) for 60 min. The cells were stained with PE-Isotype or PE-MARCO. Cell surface MARCO on the AMϕ was determined by flow cytometry. The graph depicts mean ± SEM of MARCO MFI, n=3. Statistical analysis using two-way ANOVA, Interaction $p = 0.0365$. Tukey's multiple comparisons test shows that Control/siNC vs. Control/siMARCO, $p = 0.0365$; *E. coli*/siNC vs. *E. coli*/siMARCO, $p = 0.0005$. (**E**) AMϕ were transfected with siNC or siMARCO for 36 h, and were then treated with Alexa Fluor 488- conjugated *E. coli* (MOI=4) for 60 min. The AMϕ phagocytosis of *E. coli* was measured by flow cytometry. The graph depicts mean ± SEM of intracellular Alexa Fluor 488-conjugated *E. coli* MFI, n=3. Statistical analysis using two-way ANOVA, Interaction $p < 0.0001$. Tukey's multiple comparisons test shows that *E. coli*/siNC vs. *E. coli*/siMARCO, $p < 0.0001$. (**F**) AMϕ were treated with *E. coli* (MOI=4) for 60 min. The cells were then stained with PE-Isotype, PE-MARCO or PE-FcγRI, and cell surface MARCO or FcγRI were detected by flow cytometry. The graph depicts mean ± SEM of MFI of MARCO or FcγRI, n=3. Statistical analysis using independent-samples two-tailed Student's *t*-test. MARCO/Control vs. MARCO/siMARCO, $p < 0.05$. (**G**) AMϕ were transfected with siNC or siMARCO for 36 h, and then were treated with latex beads-rabbit IgG-PE complex in 1/100 (v/v) for up to 2 hours. The intracellular latex beads-rabbit IgG-PE complex were measured by flow cytometry. The graph depicts mean ± SEM of MFI, n=3. Statistical analysis using two-way ANOVA, Interaction $p = 0.8631$. Tukey's multiple comparisons test shows that 1h/siNC vs. 1h/siMARCO, $p = 0.9784$; 2h/siNC vs. 2h/siMARCO, $p > 0.9999$. The asterisks indicate that $*p < 0.05$ or $**p < 0.01$. NS, no significant difference.

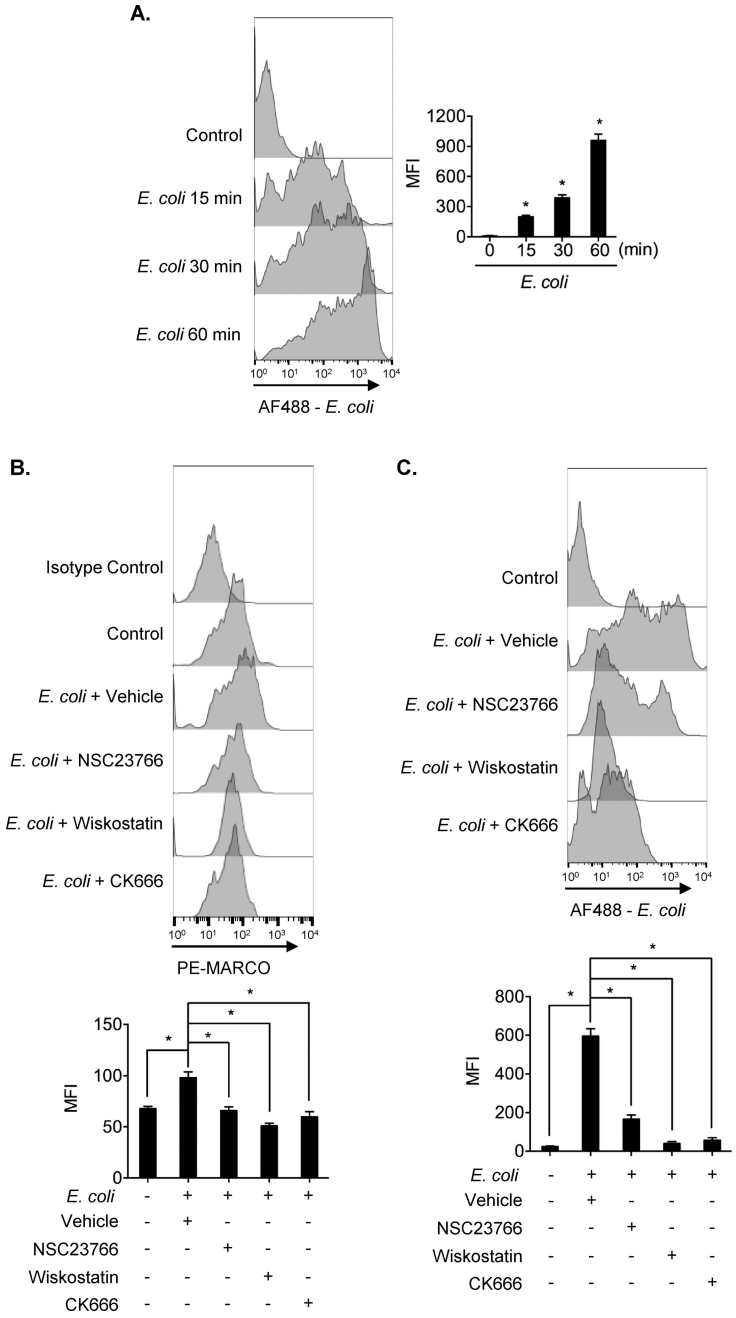

Figure 3. Actin polymerization signaling mediates MARCO cell surface expression and phagocytosis of *E. coli*

(**A)** AMϕ were treated with Alexa Fluor 488-conjugated *E. coli* (MOI=4) for 0 to 60 min, and phagocytosis of *E. coli* were measured by flow cytometry and expressed as MFI. The graph illustrates mean ± SEM of MFI of intracellular Alexa Fluor 488-conjugated *E. coli*, n=3. Statistical analysis using one-way ANOVA, over all ANOVA $p = 0.0089$. Tukey's multiple comparisons test shows that *E. coli*/15min vs. Control, $p = 0.0121$; *E. coli*/30min vs. Control, $p = 0.0176$; *E. coli*/60min vs. Control, $p = 0.0109$. (**B**) AMϕ were pretreated with Vehicle (DMSO) or NSC23766 (Rac1 inhibitor, 30 μM), Wiskostatin (N-WASP inhibitor, 30 μM), or CK666 (Arp2/3 complex inhibitor, 30 μM) for 20 min followed by treatment with *E.*

coli (MOI=4) for 60 min. Cells were then stained with PE-Isotype or PE-MARCO, and cell surface MARCO was measured by flow cytometry and expressed as MFI. The graph shows mean ± SEM of MARCO MFI, n=3. Statistical analysis using one-way ANOVA, over all ANOVA $p = 0.0035$. Tukey's multiple comparisons test shows that *E. coli*/Vehicle vs. Control, $p = 0.0409$; *E. coli*/NSC23766 vs. *E. coli*/Vehicle, $p = 0.0231$; *E. coli*/Wiskostatin vs. *E. coli*/Vehicle, $p = 0.0281$; *E. coli* /CK666 vs. *E. coli*/Vehicle, $p = 0.0452$. (**C**) AMϕ were pretreated with Vehicle (DMSO) or NSC23766 (Rac1 inhibitor, 30 μM), Wiskostatin (N-WASP inhibitor, 30 μM), or CK666 (Arp2/3 complex inhibitor, 30 μM) for 20 min. The cells were then treated with Alexa Fluor 488-conjugated *E. coli* (MOI=4) for 60 min followed by the measurement of intracellular Alexa Fluor 488-conjugated *E. coli* by flow cytometry and expressed as MFI. The graph shows mean ± SEM of intracellular MFI of Alexa Fluor 488-conjugated *E. coli*, n=3. Statistical analysis using one-way ANOVA, over all ANOVA $p = 0.0014$. Tukey's multiple comparisons test shows that *E. coli*/Vehicle vs. Control, $p = 0.0118$; *E. coli*/NSC23766 vs. *E. coli*/Vehicle, $p = 0.0157$; *E. coli*/Wiskostatin vs. *E. coli*/Vehicle, $p = 0.0115$, *E. coli*/CK666 vs. *E. coli*/Vehicle, $p = 0.0267$. The asterisk indicates that $*p < 0.05$.

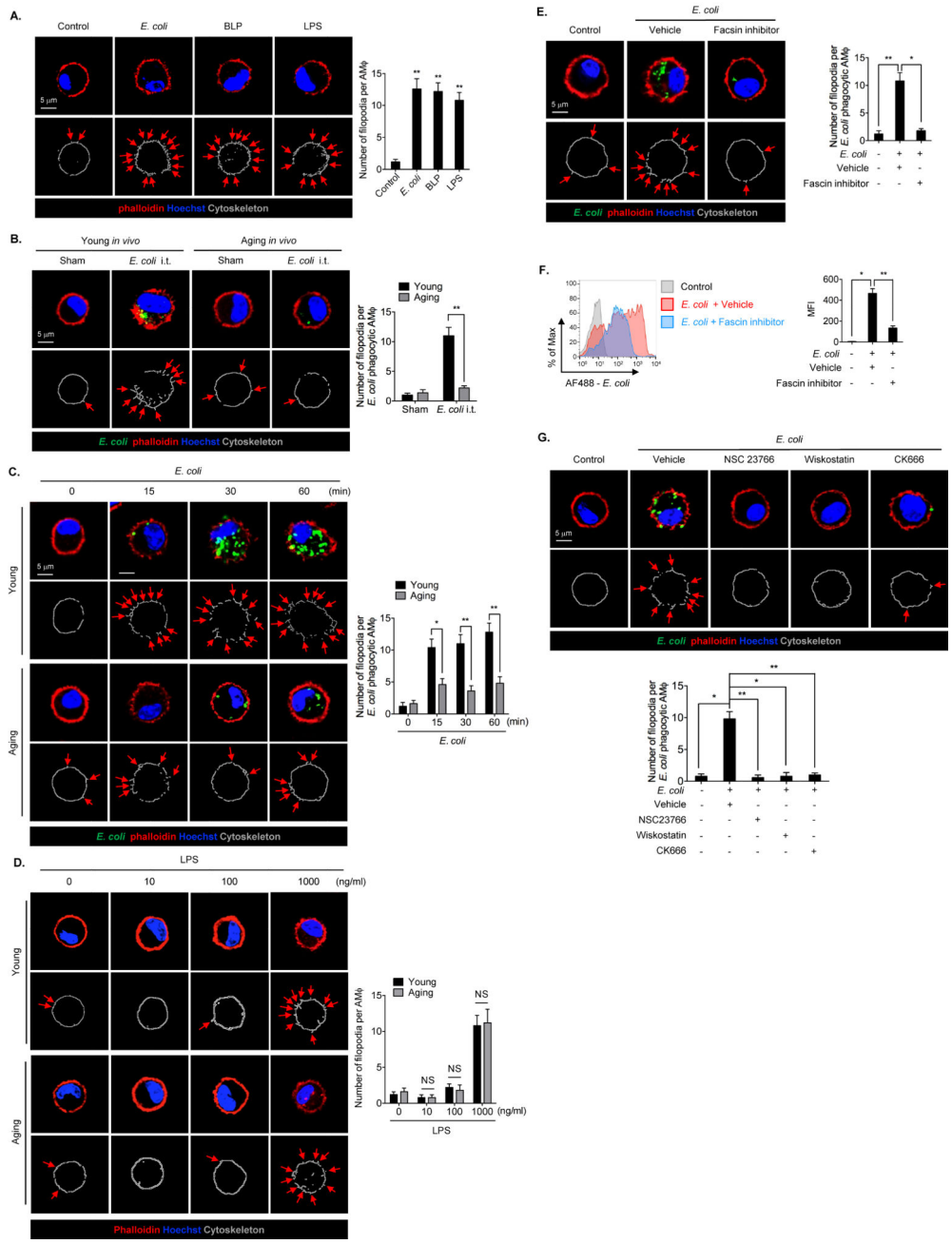

Figure 4. Aging impairs AMϕ filopodia formation and decreases phagocytosis of *E. coli*

(**A**) Confocal images show AMϕ filopodia formation. AMϕ were treated with *E. coli* (MOI=4), BLP (1 μg/ml), or LPS (1 μg/ml) for 1 h, and stained with phalloidin (for F-actin) and Hoechst (nuclear stain). The phalloidin staining was outlined by using software Image J. The arrows indicate the filopodia on AMϕ. The graph depicts mean ± SEM of number of the filopodia in AMϕ, n=5. Statistical analysis using one-way ANOVA, over all ANOVA p = 0.0028. Tukey's multiple comparisons test shows that *E. coli* vs. Control, p =0.0061; BLP vs. Control, p =0.0019; LPS vs. Control, p =0.0089. (**B**) Confocal images show AMϕ filopodia formation in young and aging mice. Young and aging mice were treated with

Alexa Fluor 488-conjugated *E. coli* (4×10^8 bacteria cells/kg B.W. i.t.) for 30 min, and AMϕ were then collected from BALF from the mice, and stained with phalloidin and Hoechst. The phalloidin staining was outlined by using software Image J. The arrows indicate the filopodia in AMϕ. The graph depicts mean ± SEM of the number of filopodia in AMϕ. n=5. Statistical analysis using two-way ANOVA, Interaction $p < 0.0001$. Tukey's multiple comparisons test shows that Young/*E. coli* vs. Sham, $p < 0.0001$; Young/*E. coli* vs. Age/*E. coli*, $p < 0.0001$. (**C**) Confocal images showing dynamic changes in filopodia formation in young and aging AMϕ following the treatment of Alexa Fluor 488 conjugated *E. coli* (MOI=4). The AMϕ were stained with phalloidin and Hoechst, and the phalloidin staining was outlined by using software Image J. The arrows indicate the filopodia. The graph depicts mean ± SEM of the numbers of filopodia on the AMϕ that phagocytosed *E. coli*, n=5. Statistical analysis using two-way ANOVA, Interaction $p = 0.0013$. Tukey's multiple comparisons test shows that Young/15min vs. Age/15min, $p = 0.0104$; Young/30min vs. Age/30min, $p = 0.0006$; Young/60min vs. Age/60min, $p = 0.0002$. (**D**) Confocal images show AMϕ filopodia formation in young and aging AMϕ. Young and aging AMϕ were treated with 0 to 1000 ng/ml LPS for 1 h, and stained with phalloidin and Hoechst. The phalloidin staining was outlined by using software Image J. The arrows indicate the filopodia in AMϕ. The graph depicts mean ± SEM of the number of filopodia in AMϕ. n=5. Statistical analysis using two-way ANOVA, Interaction $p = 0.9686$. Tukey's multiple comparisons test shows that 10/Young vs. 10/Aging, $p > 0.9999$; 100/Young vs. 100/Aging, $p > 0.9999$; 1000/Young vs. 1000/Aging, $p > 0.9999$. (**E** and **F**) AMϕ were pretreated with Vehicle or Fascin inhibitor (25 μM) for 20 min followed by stimulation with Alexa Fluor 488-conjugated *E. coli* (MOI=4) for 60 min. (**E**) AMϕ were then stained with phalloidin and Hoechst, and phalloidin staining was outlined by using software Image J. The arrows indicate the filopodia. The graph depicts mean ± SEM of the numbers of filopodia on the AMϕ that phagocytosed *E. coli*, n=5. Statistical analysis using one-way ANOVA, over all ANOVA $p = 0.0021$. Tukey's multiple comparisons test shows that *E. coli*/Vehicle vs. Control, $p = 0.003$; *E. coli*/Vehicle vs. *E. coli*/Fascin inhibitor, $p = 0.0134$. (**F**) Phagocytosis of Alexa Fluor 488- conjugated *E. coli* determined by flow cytometry. The graph depicts mean ± SEM of the MFI of Alexa Fluor 488-conjugated *E. coli*, $n=3$. Statistical analysis using one-way ANOVA, over all ANOVA $p = 0.0083$. Tukey's multiple comparisons test shows that *E. coli*/Vehicle vs. Control, $p = 0.0162$; *E. coli*/Vehicle vs. *E. coli*/Fascin inhibitor, $p = 0.0090$. (**G**) AMϕ were pretreated with Vehicle (DMSO) or NSC23766 (30 μM), Wiskostatin (30 μM), or CK666 (30 μM) for 20 min, then the cells were stimulated with Alexa Fluor 488-conjugated *E. coli* (MOI=4) for 30 min. The AMϕ were stained with phalloidin and Hoechst. The phalloidin staining was outlined by using software Image J. The arrows indicated the filopodia in AMϕ. The graph depicts mean ± SEM of number of filopodia in AMϕ n=5. Statistical analysis using one-way ANOVA, over all ANOVA $p = 0.0004$. Tukey's multiple comparisons test shows that *E. coli*/Vehicle vs. Control, $p = 0.0108$; *E. coli*/NSC23766 vs. *E. coli*/Vehicle, $p = 0.0093$; *E. coli*/Wiskostatin vs. *E. coli*/Vehicle, $p = 0.0172$; *E. coli*/CK666 vs. *E. coli*/Vehicle, $p = 0.0097$. The asterisks indicate that $*p < 0.05$ or $**p < 0.01$. NS, no significant difference.

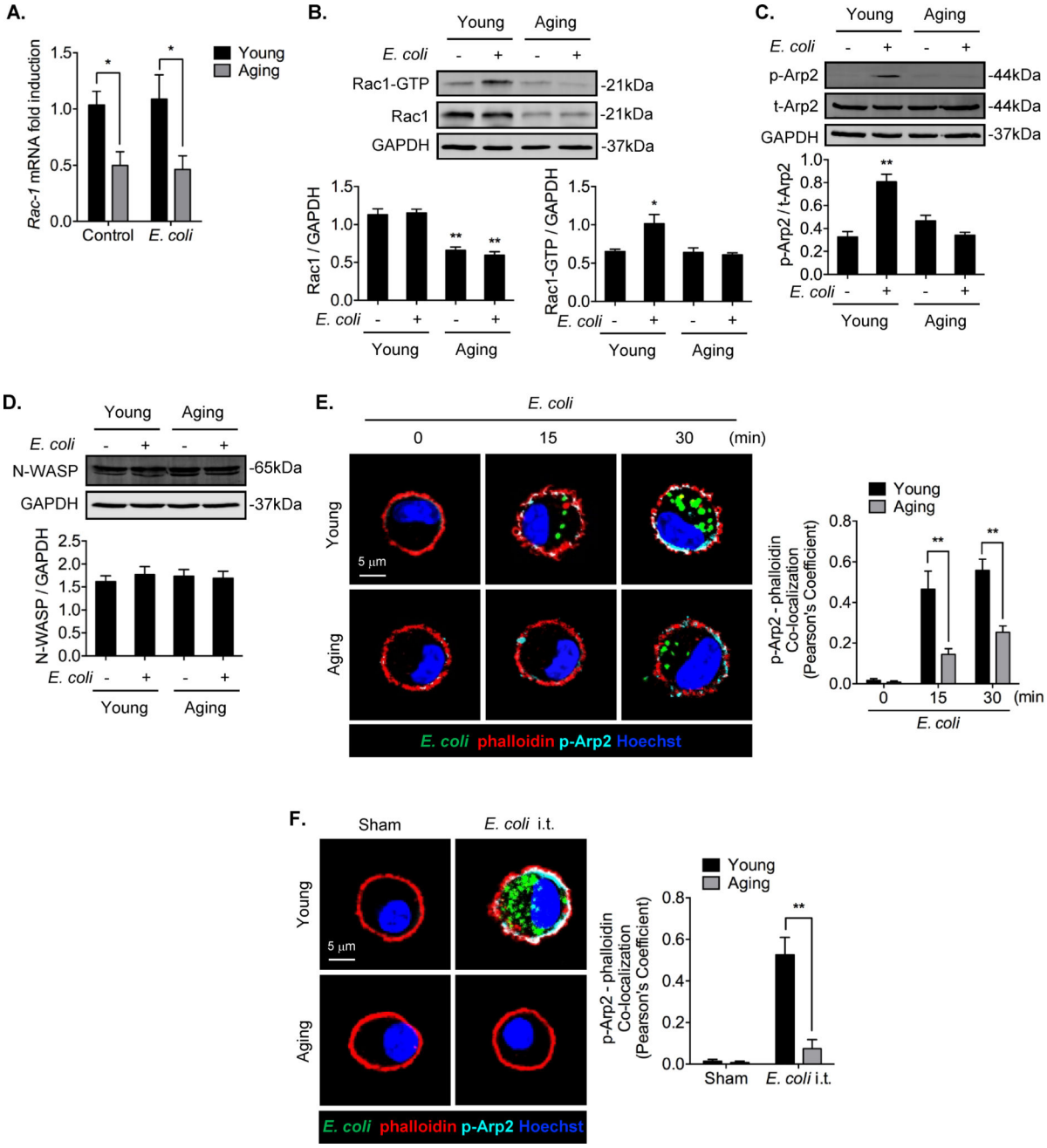

Figure 5. Aging suppresses Rac1 expression and decreases Rac1-GTP level

(**A**) Young and aging AMϕ were treated with *E. coli* (MOI=4) for 30 min. The *Rac1* mRNA level was measured by RT-QPCR. The graph depicts mean ± SEM of *Rac1* mRNA fold induction, n=3. Statistical analysis using two-way ANOVA, Interaction $p = 0.7593$. Tukey's multiple comparisons test shows that Young/Control vs. Age/Control, $p = 0.0457$; Young/*E. coli* vs. Age/*E. coli*, $p = 0.0363$. (**B**) Young and aging AMϕ were treated with or without *E. coli* (MOI=4) for 30 min, the Rac1-GTP was enriched via Rac1/cdc42 activation magnetic beads and measured by Western Blot. The left graph shows mean ± SEM of Rac1/GAPDH intensity fold induction, n=3. Statistical analysis using two-way ANOVA, Interaction $p =$

0.4492. Tukey's multiple comparisons test shows that Young/Control vs. Age/Control, p = 0.0015; Young/*E. coli* vs. Age/*E. coli*, p = 0.0005. The right graph shows mean ± SEM of Rac1-GTP/GAPDH intensity fold induction, n=3. Statistical analysis using two-way ANOVA, Interaction p = 0.0225. Tukey's multiple comparisons test shows that Young/Control vs. Young/*E. coli*, p = 0.0256, Young/*E. coli* vs. Age/*E. coli*, p = 0.0142. (**C**) Young and aging AMϕ were treated with or without *E. coli* (MOI=4) for 30 min, the total Arp2 and its phosphorylated form were measured by Western Blot. The graph depicts mean ± SEM of p-Arp2/t-Arp2 intensity fold induction, n=3. Statistical analysis using two-way ANOVA, Interaction p = 0.0003. Tukey's multiple comparisons test shows that Young/Control vs. Young/*E. coli*, p = 0.0006, Young/*E. coli* vs. Age/*E. coli*, p = 0.0007. (**D**) Young and aging AMϕ were treated with or without *E. coli* (MOI=4) for 30 min, the N-WASP was detected by Western Blot. The graph shows mean ± SEM of N-WASP/GAPDH intensity fold induction, n=3. Statistical analysis using two-way ANOVA, Interaction p = 0.5214. (**E**) Confocal immunofluorescence images showing colocalization of p-Arp2 (cyan), phalloidin (red), and Hoechst (blue) in young and aging AMϕ, which were treated with Alexa Fluor 488-conjugated *E. coli* (MOI=4) for 0 to 30 min. The graph depicts mean ± SEM of Pearson's Coefficient of p-Arp2 and phalloidin, n=3. Statistical analysis using two-way ANOVA, Interaction p = 0.0089. Tukey's multiple comparisons test shows that 15min/Young vs. 15min/Aging, p = 0.0039; 30 min/Young vs. 30 min/Aging, p = 0.0058. (**F**) Young and aging mice were administered with Alexa Fluor 488-conjugated *E. coli* (4×10^8 bacteria/kg B.W., i.t) for 30 min. The images show the colocalization of p-Arp2 (cyan), phalloidin (red), and Hoechst (blue) in young and aging AMϕ. The graphs show mean ± SEM of Pearson's Coefficient of p-Arp2 and phalloidin, n=3. Statistical analysis using two-way ANOVA, Interaction p = 0.0016. Tukey's multiple comparisons test shows that *E. coli*/Young vs. *E. coli*/Aging, p = 0.0007. The asterisks indicate that $*p < 0.05$ or $**p < 0.01$.